Asymptotic-preserving schemes for kinetic-fluid modeling of disperse two-phase flows

Thierry Goudon [a,1], Shi Jin [b,c,*], Jian-Guo Liu [d], Bokai Yan [e]

[a] *Labo. J. A. Dieudonne UMR 7351, CNRS & Université Nice Sophia Antipolis, France*
[b] *Department of Mathematics, Institute of Natural Sciences, and Ministry of Education Key Laboratory of Scientific and Engineering Computing, Shanghai Jiao Tong University, Shanghai 200240, China*
[c] *Department of Mathematics, University of Wisconsin-Madison, Madison, WI 53706, USA*
[d] *Department of Physics and Department of Mathematics, Duke University, Durham, NC 27708, USA*
[e] *Department of Mathematics, University of California, Los Angeles, CA 90095, USA*

ABSTRACT

We consider a system coupling the incompressible Navier–Stokes equations to the Vlasov–Fokker–Planck equation. Such a problem arises in the description of particulate flows. We design a numerical scheme to simulate the behavior of the system. This scheme is asymptotic-preserving, thus efficient in both the kinetic and hydrodynamic regimes. It has a numerical stability condition controlled by the non-stiff convection operator, with an implicit treatment of the stiff drag term and the Fokker–Planck operator. Yet, consistent to a standard asymptotic-preserving Fokker–Planck solver or an incompressible Navier–Stokes solver, only the conjugate–gradient method and fast Poisson and Helmholtz solvers are needed. Numerical experiments are presented to demonstrate the accuracy and asymptotic behavior of the scheme, with several interesting applications.

© 2013 Elsevier Inc. All rights reserved.

1. Introduction

This paper is concerned with the simulation of a system of PDEs describing the evolution of disperse two-phase flows. While these flows can be modeled by a continuum description for all phases [1] we adopt here a kinetic-fluid modeling [2]. Such models are applicable to suspensions of solids as well as droplets. We use a kinetic description for the particulate phase and a hydrodynamic one for the underlying continuous fluid phase. Typical applications cover the dynamics of sprays [3–6], particulate flows in fluidized beds [7], the calibration of fire prevention devices [8], environmental studies on pollutant transport [9–14], combustion theory [2,15,16] and engine design [17].

There exists a large variety of kinetic-fluid models, depending on the considered physical regime. Here and below, we adopt the following assumptions:

- The fluid phase is incompressible and viscous. For the sake of simplicity, we suppose that the fluid density is constant and homogeneous (see Remark 2.1 below).
- Both the fluid and particle phases are isothermal.
- We consider a single species of particles, with a given and fixed mass density and size.

- We assume there is no mass exchange between the phases, or in other words, the volume fraction occupied by the particles does not influence significantly the fluid density. According to O'Rourke [2], it corresponds to the so-called Thin Sprays modeling.
- Particles are subject to Brownian motion: according to Einstein [18,19] it leads to diffusion with respect to the velocity variable in the equation for the particle distribution function.
- Each phase exerts an influence on the other phase through drag forces. Models for the drag forces are developed through experimental investigation and can have quite intricate expressions. Here we shall use the simplest Stokes formula where the drag force is proportional to the relative velocity $(v - u)$. An interesting derivation through homogenization arguments is discussed in [20].

Then, the flows are described by the fluid velocity field $u(t, x) \in \mathbb{R}^N$, depending on time $t \geqslant 0$ and space $x \in \mathbb{R}^N$, and the particle distribution function $f(t, x, v)$, which additionally depends on the (particle) velocity variable $v \in \mathbb{R}^N$. The evolution of the density f is governed by

$$\partial_t f + v \cdot \nabla_x f = \frac{1}{\varepsilon} L_u f + \nabla_x \Phi \cdot \nabla_v f, \tag{1}$$

where we have set

$$L_u f = \nabla_v \cdot ((v - u)f + \nabla_v f). \tag{2}$$

A derivation of such an operator for particles in inhomogeneous flows is discussed in [21]. The evolution of the fluid obeys the Incompressible Navier–Stokes system

$$\begin{cases} \partial_t u + \nabla_x \cdot (u \otimes u) + \nabla_x p - \Delta_x u = \frac{1}{\varepsilon} \kappa \int (v - u)f \, \mathrm{d}v, \\ \nabla_x \cdot u = 0, \end{cases} \tag{3}$$

with $\kappa > 0$ a coupling constant that depends on the physical properties of the two phases.

The two phases are subject to external forces, embodied into the potential Φ. Of course, in the momentum Eq. (3), the external force term is incorporated within the pressure. Note however that the strength and the orientation of the external force might be different for the two phases. A relevant example is given by gravity driven flows where $\nabla_x \Phi$ is proportional to g, the gravitational acceleration. For the particles, the coefficient is $\eta_P = (1 - \rho_F/\rho_P)$ which accounts for the buoyancy force, with ρ_F and ρ_P (typical) densities of the fluid and the particles, respectively. The system (1)–(3) is written here in dimensionless form. The scaling parameter ε is associated to the Stokes settling time

$$\frac{2\rho_P a^2}{9\mu}$$

with μ the dynamic viscosity of the fluid, a the typical radius of the particles. We refer e.g. to [22,23] for further details on the scaling issues.

The goal of the present paper is the design of a performing numerical scheme, able to handle different regimes, from $\varepsilon = O(1)$ (the kinetic regime) to $\varepsilon \ll 1$ (the hydrodynamic regime). As will be detailed below, in the hydrodynamic regime, the particle distribution function relaxes to the Maxwellian $\frac{n(t,x)}{(2\pi)^{N/2}} e^{-|v-u(t,x)|^2/2}$ and the limiting system for particle density n and particle macroscopic velocity u, which coincides to the fluid velocity, looks like the non homogeneous incompressible Navier–Stokes system, see (10) and (11).

Existence of weak solutions of system (1)–(3) has been investigated in [24] by fixed point methods and the theory has been revisited in [25] by using compactness techniques. Definitely, a difficulty relies on the construction of approximate solutions that preserve the conservation/dissipation properties of the model. We also refer to [26] for the analysis of compressible models. Smooth solutions close to equilibrium are studied in [27], see also [28] for a similar analysis of macroscopic models. The analysis of the asymptotics $\varepsilon \to 0$ in (1)–(3) is due to [29] by means of relative entropy methods, see also [30]. It is also worth mentioning related works like the local existence of smooth solutions for the case without velocity-diffusion [31], several studies of coupling with the Euler system (i.e. viscosity is sensible only at the scale of the particles) [23,32,33] and systems with energy exchanges [34–36].

This work is organized as follows. In Section 2 we detail a few basic facts about the system (1)–(3) and the regime $\varepsilon \to 0$. In Section 3 we detail the construction of the numerical scheme. Our method takes place among the so-called "Asymptotic Preserving Schemes", a terminology coined in [37]. It means that the scheme is suitable for the kinetic equation in such a way that letting ε go to 0 while holding the mesh size and time step fixed, the scheme becomes a suitable scheme for the limiting equations. In particular, the stability constraints do not degenerate in the asymptotic regime. We refer to [38] and references therein for a recent review on the AP schemes and their applications. Roughly speaking the idea consists in evaluating implicitly the stiff terms of the equation. Here, it will require to invert the Fokker–Planck operator (2). To this end, we will follow the discretization introduced in [39]. Furthermore, our formulation of the scheme follows the framework of the projection method (see Chorin [40,41], Temam [42]), in the sense that only fast Helmholtz or Poisson solvers are needed, even with the implicit, nonlocal coupling terms between particles and the fluid. This is most natural when the incompressible fluid equations are solved by the projection method. The Fokker–Planck solver here, on the other hand,

has a computational cost and complexity comparable to the previously developed AP scheme without the coupling to the fluid equation [39]. Both first and second order schemes are presented in this framework. Section 4 is devoted to the results of numerical simulations for checking accuracy, asymptotic behavior as well as some applications.

2. Hydrodynamic limit

Let us briefly recall some basic facts about the system (1)–(3) and the regime $\varepsilon \to 0$. The key remark, observed in [43,29], relies on the following energy-entropy dissipation property

$$\frac{d}{dt}\left(\kappa \int_{\mathbb{R}^N \times \mathbb{R}^N} f\big(1 + \Phi + v^2/2 + \ln(f)\big)\,dv\,dx + \int_{\mathbb{R}^N} |u|^2/2\,dx\right) + \int_{\mathbb{R}^N} |\nabla_x u|^2\,dx + \frac{\kappa}{\varepsilon} \int_{\mathbb{R}^N \times \mathbb{R}^N} |(v - u)\sqrt{f} + 2\nabla_v\sqrt{f}|^2\,dv\,dx = 0. \tag{4}$$

A similar relation holds when the problem is set on a bounded smooth domain Ω with reasonable boundary conditions. For instance we can assume no–slip of the fluid

$$u|_{\partial\Omega} = 0 \tag{5}$$

and specular reflection of the particles

$$\gamma^- f(t, x, v) = \gamma^+ f(t, x, v - 2v \cdot \hat{v}(x)\hat{v}(x)), \tag{6}$$

where $\hat{v}(x)$ stands for the unit outer normal at point $x \in \partial\Omega$ and $\gamma^\pm$ denote the trace operators on the set

$$\{(t, x, v) \in (0, \infty) \times \partial\Omega \times \mathbb{R}^N, \quad \pm v \cdot \hat{v}(x) > 0\}.$$

We refer to further comments in [23]. It is worth rewriting the Fokker–Planck operator as

$$L_u f = \nabla_v \cdot \left(M_u \nabla_v\left(\frac{f}{M_u}\right)\right), \quad M_u(v) = \frac{1}{(2\pi)^{N/2}} \exp\left(-\frac{|v - u(t,x)|^2}{2}\right).$$

As ε goes to 0, since the Fokker–Planck operator is penalized, we expect that f makes $L_u f$ (and the dissipation term in (4)) vanish which means that f becomes proportional to the Maxwellian centered to the fluid velocity

$$f(t, x, v) \simeq n(t, x)M_{u(t,x)}.$$

Hence the question is to identify the equation satisfied as $\varepsilon \to 0$ by the particles density n and the velocity u.

To this end, let us write the equations satisfied by the moments

$$n(t, x) = \int_{\mathbb{R}^N} f(t, x, v)\,dv, \quad J(t, x) = \int_{\mathbb{R}^N} vf(t, x, v)\,dv.$$

Then one has

$$\partial_t n + \nabla_x \cdot J = 0, \tag{7}$$

$$\partial_t J + \nabla_x \mathbb{P} + n\nabla_x \Phi = -\frac{1}{\varepsilon}(J - nu) \tag{8}$$

where

$$\mathbb{P}(t, x) = \int_{\mathbb{R}^N} v \otimes vf(t, x, v)\,dv.$$

Combined to (3) one obtains

$$\partial_t(u + \kappa J) + \nabla_x \cdot (u \otimes u + \kappa\mathbb{P}) + \nabla_x p + \kappa n\nabla_x \Phi = \Delta_x u. \tag{9}$$

Accordingly, when J and $\mathbb{P}$ are asymptotically defined by the moments of the Maxwellian nM_u, one is led to

$$J \simeq nu, \quad \mathbb{P} \simeq nu \otimes u + n\mathbb{I}.$$

Inserting this ansatz into (9) one arrives at

$$\partial_t((1 + \kappa n)u) + \nabla_x \cdot ((1 + \kappa n)u \otimes u) + \nabla_x(p + \kappa n) + \kappa n\nabla_x \Phi = \Delta_x u, \tag{10}$$

where the velocity is still required to be divergence free while for the density of particles

$$\partial_t n + \nabla_x \cdot (nu) = 0. \tag{11}$$

The system (10) and (11) is (up to the gravity term) nothing but the incompressible Navier–Stokes system for the composite and inhomogeneous density $(1 + \kappa n)$. Of course a rigorous justification of the convergence statement presents technical

difficulties, due to the nonlinear passages to the limit it requires, in particular with the product $nu \otimes u$. We refer to [29] for a proof based on relative entropy arguments and to [26,30,23] where related questions are discussed.

Remark 2.1. Note that the problem does not simplify if we start with the Stokes equation for the fluid instead of (3), because the convection term in the limit equation comes anyway from the kinetic pressure $\mathbb{P}$. We point out also that it makes sense to consider from the beginning that the fluid density $\rho(t, x)$ is non homogeneous. In such a case (3) is replaced by

$$\partial_t \rho + \nabla_x \cdot (\rho u) = 0,$$

$$\partial_t (\rho u) + \nabla_x \cdot (\rho u \otimes u) + \nabla_x p + \eta_F \rho \nabla_x \tilde{\Phi} = \Delta_x u + \frac{1}{\varepsilon} \kappa \int_{\mathbb{R}^N} (v - u) f \, dv,$$

coupled to the divergence free constraint $\nabla_x \cdot u = 0$. Here $\nabla_x \tilde{\Phi} = \frac{1}{\eta_P} \nabla_x \Phi = g$. Note the coefficient η_F, potentially different from η_P, characterizes the effect of the external forces on the fluid. The limiting problem will be of the same type for the composite density $\rho + \kappa n$; namely one obtains as $\varepsilon \to 0$

$$\partial_t \rho + \nabla_x \cdot (\rho u) = 0 = \partial_t n + \nabla_x \cdot (nu) = 0,$$

$$\partial_t ((\rho + \kappa n)u) + \nabla_x \cdot ((\rho + \kappa n)u \otimes u) + \nabla_x (p + \kappa n) + (\eta_F \rho + \eta_P n)\nabla_x \tilde{\Phi} + \Delta_x u = 0,$$

$$\nabla_x \cdot u = 0.$$

Adaptation of our numerical method to fully non homogeneous flows is discussed in a forthcoming work [44].

3. An AP scheme for the kinetic-fluid coupling system

As announced in the Introduction, we wish to construct a numerical scheme for (1)–(3), with the specific request to capture the asymptotic regime $\varepsilon \to 0$ efficiently. In particular, as ε goes to 0, the scheme should become a robust solver for the limit system (10), (11). Furthermore, the asymptotic regime should not introduce prohibitive numerical constraints, by having the stability condition independent of ε. A scheme that fulfills these requirements is said Asymptotic Preserving [37,45,38]. Roughly speaking, the idea is to evaluate implicitly the stiff terms in the equations, namely the drag force in (3) and the Fokker–Planck operator in (1). The key point of the method that provides the AP property to the scheme relies on a convenient time splitting which allows to compute implicitly the stiff terms efficiently. Recall that an AP scheme for the Fokker–Planck equation, developed in [39], relies just on a conjugate gradient method for the implicit Fokker–Planck operator, while a typical incompressible Navier–Stokes solver, such as the projection method, requires a fast Poisson or Helmholtz solver. For the problem under study, even if more implicit coupling terms are involved than the problems studied previously, our AP schemes do not require more than the conjugate gradient method and a fast Poisson or Helmholtz solver.

3.1. Projection method for INS system with variable fluid density

In this section we recall the projection method for the incompressible Navier–Stokes (INS) system with variable fluid density with no–slip boundary condition:

$$\begin{cases} \partial_t \rho + \nabla_x \cdot (\rho u) = 0, \\ \partial_t (\rho u) + \nabla_x \cdot (u \otimes u) + \nabla_x p - \Delta u = S, \\ \nabla_x \cdot u = 0, \\ u(t, x) = 0, \quad \text{on } \partial\Omega. \end{cases} \tag{12}$$

Here we can assume S is a stiff source term.

Although the fluid is modeled by (3) with constant fluid density, we have a good reason to start with the review of the projection scheme for (12). That is, the limit system (10), (11) itself is a variable density INS system. We want our scheme automatically becomes a projection method for (10), (11) as $\varepsilon \to 0$.

The projection method for INS system with constant fluid density was first introduced by Chorin ([40,46,41]) and Temam ([42]). The extensions to second order have been studied a lot, for example, in [47–49]. It is also generalized to (12), the INS system with variable density, for example, in [50–53]. In this section we focus on the temporal discretization. The space derivative is assumed to be continuous at this moment. We leave the spatial discretization to the end of this section.

3.1.1. A first order method
A first order projection method can be summarized as

$$\begin{cases} \frac{\rho^{k+1} - \rho^k}{\Delta t} + \nabla_x \cdot (\rho^k u^k) = 0, \\ \frac{\rho^{k+1} u^* - \rho^k u^k}{\Delta t} + \nabla_x \cdot (\rho^k u^k \otimes u^k) - \Delta_x u^* = S^*, \\ \frac{u^{k+1} - u^*}{\Delta t} + \frac{1}{\rho^{k+1}} \nabla_x p^{k+1} = 0, \quad \text{with } \nabla_x \cdot u^{k+1} = 0. \end{cases} \tag{13}$$

The system is solved with no-slip boundary condition for u^*, Neumann boundary condition for p^{k+1},

$$u^* = u^k \frac{\partial p^{k+1}}{\partial \hat{v}} = 0, \quad \text{on } \partial \Omega. \tag{14}$$

The momentum equation is split into a viscosity step (for u^*) and a projection step (for u^{k+1}). The viscosity step needs a Helmholtz solver. Similarly to the projection method for the constant density INS system, the projection step is solved in two steps. First the pressure p^{k+1} is computed by taking the divergence of both sides,

$$\nabla_x \cdot \left(\frac{1}{\rho^{k+1}} \nabla_x p^{k+1} \right) = \frac{1}{\Delta t} \nabla_x \cdot u^*,$$

where a variable coefficient Poisson solver is needed. Then u^{k+1} is updated via

$$u^{k+1} = u^* + \frac{\Delta t}{\rho^{k+1}} \nabla_x p^{k+1}.$$

This is a direct generalization of Chorin-Temam projection method to the system (12).

3.1.2. A second order method

The second order projection methods for (12) have been studied in [50], with a Crank–Nicolson type stiff term. However, to obtain an AP scheme, we hope the stiff term is solved fully implicitly. Illustrated by [52], we give the following BDF based second order pressure incremental (also called pressure correction) projection method:

$$\begin{cases} \frac{3\rho^{k+1} - 4\rho^k + \rho^{k-1}}{2\Delta t} + \nabla \cdot (2\rho^k u^k - \rho^{k-1} u^{k-1}) = 0, \\ \frac{3\rho^{k+1} u^* - 4\rho^k u^k + \rho^{k-1} u^{k-1}}{2\Delta t} + 2(\nabla_x \cdot (u \otimes u))^k - (\nabla_x \cdot (u \otimes u))^{k-1} + \nabla_x p^k - \Delta u^* = S^*, \\ \frac{3u^{k+1} - 3u^*}{2\Delta t} + \frac{1}{\rho^{k+1}} \nabla_x (p^{k+1} - p^k) = 0, \quad \text{with } \nabla_x \cdot u^{k+1} = 0. \end{cases} \tag{15}$$

The same boundary conditions (14) are applied. This is solved in a similar way as in the first order method.

This second order method is based on the pressure correction idea introduced in [48], which is necessary for the INS system with variable density. The viscosity part of momentum equation is solved with current pressure $\nabla_x p^k$. Then the pressure increment, $(p^{k+1} - p^k)$, is computed in the projection step.

3.2. Construction of the AP schemes

The AP scheme works in two steps. Firstly we update the macroscopic quantities n, J, u, p and secondly we update the microscopic density of particles. The former leads to invert a coupled linear system. The latter needs to invert the Fokker–Planck operator, which relies on a specific discretization to obtain an appropriate structure for using performing algorithms.

To start with, we compute the macroscopic density of particles,

$$\frac{1}{\Delta t}(n^{k+1} - n^k) = -\int v \cdot \nabla_x f^k \mathrm{d}v. \tag{16}$$

Next we solve the coupled momentum Eqs. (8) with (3), based on the projection method described in Section 3.1.1. We would like to point out that, to derive an AP scheme, one has to impose the stiff coupling term ($1/\varepsilon$ term) in both the viscosity step and the projection step.

We solve the viscosity part of momentum equations with only part of the stiff term:

$$\frac{1}{\Delta t}(J^* - J^k) = -\int v \otimes v \nabla_x f^k \mathrm{d}v - n^k \nabla_x \Phi - \frac{1-\alpha}{\varepsilon}(J^* - n^{k+1} u^*), \tag{17a}$$

$$\frac{1}{\Delta t}(u^* - u^k) - \Delta_x u^* = -\nabla_x \cdot (u^k \otimes u^k) + \frac{1-\alpha}{\varepsilon} \kappa (J^* - n^{k+1} u^*), \tag{17b}$$

where $\alpha \in (0, 1)$ is any constant. One can simply choose $\alpha = \frac{1}{2}$.

It is equivalent to solve

$$\left(\frac{1}{\Delta t} + \frac{1-\alpha}{\varepsilon + (1-\alpha)\Delta t} \kappa n^{k+1} - \Delta_x \right) u^* = \frac{u^k}{\Delta t} - \nabla_x \cdot (u^k \otimes u^k) + \frac{(1-\alpha)\kappa}{\varepsilon + (1-\alpha)\Delta t} \left(J^k - \Delta t \int v \otimes v \nabla_x f^k \mathrm{d}v - \Delta t n^k \nabla_x \Phi \right). \tag{18}$$

The no-slip boundary condition for u^* is used,

$$u^*|_{\partial \Omega} = 0. \tag{19}$$

(18) is a Helmholtz equation for u^*, which can be solved by the Preconditioned Conjugate Gradient method without difficulties (for example, see [54]). Then J^* is solved accordingly.

Next u^* is projected to the divergence free space, with the remaining stiff coupling term.

$$\frac{1}{\Delta t}(J^{**} - J^*) = -\frac{\alpha}{\varepsilon}(J^{**} - n^{k+1}u^{k+1}),$$

$$\frac{1}{\Delta t}(u^{k+1} - u^*) + \nabla_x p^{k+1} = \frac{\alpha}{\varepsilon}\kappa(J^{**} - n^{k+1}u^{k+1}). \tag{20}$$

With J^{**} canceled, one has,

$$u^{k+1} + \frac{\frac{1}{\Delta t} + \frac{\alpha}{\varepsilon}}{\frac{1}{\Delta t} + \frac{\alpha}{\varepsilon}(1 + \kappa n^{k+1})}\Delta t \nabla_x p^{k+1} = \frac{(\frac{1}{\Delta t} + \frac{\alpha}{\varepsilon})u^* + \frac{\alpha}{\varepsilon}\kappa J^*}{\frac{1}{\Delta t} + \frac{\alpha}{\varepsilon}(1 + \kappa n^{k+1})}. \tag{21}$$

Noting that u^{k+1} is divergence free, by taking the divergence of both sides, one arrives at,

$$\nabla_x \cdot \left(\frac{1}{\rho_\varepsilon^{k+1}}\nabla_x p^{k+1}\right) = \frac{1}{\Delta t}\nabla_x \cdot \left(\frac{(\frac{1}{\Delta t} + \frac{\alpha}{\varepsilon})u^* + \frac{\alpha}{\varepsilon}\kappa J^*}{\frac{1}{\Delta t} + \frac{\alpha}{\varepsilon}(1 + \kappa n^{k+1})}\right), \quad \frac{\partial p^{k+1}}{\partial \hat{v}}\Big|_{\partial\Omega} = 0, \tag{22}$$

with

$$\rho_\varepsilon^{k+1} := \frac{\frac{1}{\Delta t} + \frac{\alpha}{\varepsilon}(1 + \kappa n^{k+1})}{\frac{1}{\Delta t} + \frac{\alpha}{\varepsilon}}, \tag{23}$$

where the dependence on Δt and α is omitted in the notation, for the sake of simplicity.

p^{k+1} is solved from Eq. (22) by a Conjugate Gradient method. Then u^{k+1} is obtained from (21). Finally f^{k+1} is solved based on the kinetic Eq. (1), with a fully implicit Fokker–Panck operator

$$\frac{f^{k+1} - f^k}{\Delta t} + v \cdot \nabla_x f^k - \nabla_x \Phi \cdot \nabla_v f^k = \frac{1}{\varepsilon}L_{u^{k+1}}f^{k+1}, \tag{24}$$

where

$$L_{u^{k+1}}f^{k+1} = \nabla_v \cdot ((v - u^{k+1})f^{k+1} + \nabla_v f^{k+1}).$$

Then J^{k+1} is updated by taking the first moment of f^{k+1}.

This is a *predictor–corrector* method for the kinetic Eq. (1). One first predicts the momentum at t^{k+1} by solving for u^*. Then the divergence free velocity u^{k+1} is derived and the momentum J^{k+1} at t^{k+1} is corrected accordingly. The only constraint on time step is the CFL condition from the transport part of kinetic Eq. (1), i.e. $\Delta t \leqslant \frac{\Delta x}{\max|v|}$, with Δx the space mesh size.

3.3. A second order scheme

However, any constant $\alpha \in (0, 1)$ will result in a first order time splitting. To derive a second order scheme, we start with a lemma on a toy model.

Lemma 3.1. *The ODE equation*

$$\frac{du}{dt} = f(u)$$

can be solved by

$$\frac{3u^* - 4u^k + u^{k-1}}{2\Delta t} = (1 - \alpha)f(u^*),$$

$$\frac{3u^{k+1} - 3u^*}{2\Delta t} = \alpha f(u^{k+1}).$$

The method is second order if $\alpha = 0, 1$. Furthermore, the second order is also achieved if

$$\alpha = O(\Delta t), \quad \text{or } 1 - \alpha = O(\Delta t).$$

The proof is straightforward if one studies the local truncation error. The case $\alpha = O(\Delta t)$ is what we need.

Now we generalize the first order scheme (16), (17a), (17b), (18)–(24) to second order. The convergence order can be improved by the following techniques.

- The time derivative terms are approximated by a second order BDF method, i.e.,

$$\partial_t a(t^{k+1}) \approx \frac{3a^{k+1} - 4a^k + a^{k-1}}{2\Delta t};$$

- The transport terms are approximated by extrapolation from previous two steps, i.e.,

$$b(t^{k+1}) \approx 2b^k - b^{k-1};$$

- The stiff terms are implicitly evaluated at t^{k+1};
- Take $\alpha = O(\Delta t)$ in the splitting of stiff terms.
- Pressure incremental technique. The viscosity step in momentum equation is solved with pressure at current step. Then the projection step computes the pressure increment.

We describe the detailed scheme now. For simplicity we denote

$$a^\dagger = 2a^k - a^{k-1}.$$

First, the macroscopic density of particles n^{k+1} is computed by,

$$\frac{1}{2\Delta t}(3n^{k+1} - 4n^k + n^{k-1}) = -\int v \cdot \nabla_x f^\dagger \mathrm{d}v. \tag{25}$$

Next we solve the coupled momentum Eqs. (8) with (3), with part of stiff terms and pressure term at t^k,

$$\frac{1}{2\Delta t}(3J^* - 4J^k + J^{k-1}) = -\int v \otimes v \nabla_x f^\dagger \mathrm{d}v - n^\dagger \nabla_x \Phi - \frac{1-\alpha}{\varepsilon}(J^* - n^{k+1}u^*),$$
$$\frac{1}{2\Delta t}(3u^* - 4u^k + u^{k-1}) - \Delta_x u^* + \nabla_x p^k = -\nabla_x \cdot (u \otimes u)^\dagger + \frac{1-\alpha}{\varepsilon}\kappa(J^* - n^{k+1}u^*). \tag{26}$$

Again $\alpha \in (0,1)$. Illustrated by Lemma 3.1, we need $\alpha = O(\Delta t)$ to ensure the second order accuracy. We take $\alpha = \frac{\Delta t}{t_{\max}}$, where $t_{\max}$ is the final time of our simulation.

The above system can be recast as

$$\left(\frac{3}{2\Delta t} + \frac{3(1-\alpha)}{3\varepsilon + 2(1-\alpha)\Delta t}\kappa n^{k+1} - \Delta_x\right)u^* = \frac{4u^k - u^{k-1}}{2\Delta t} - \nabla_x \cdot (u \otimes u)^\dagger - \nabla_x p^k$$
$$+ \frac{1-\alpha}{3\varepsilon + 2(1-\alpha)\Delta t}\kappa\left\{4J^k - J^{k-1} - 2\Delta t\left(\int v \otimes v \nabla_x f^\dagger \mathrm{d}v + n^\dagger \nabla_x \Phi\right)\right\}. \tag{27}$$

The no-slip boundary condition for u^* is used.

Eq. (27) can be solved by the Preconditioned Conjugate Gradient method without difficulties. Then J^* is solved using (26). Next u^* is projected to the divergence free space, with pressure correction and the remaining part of stiff terms,

$$\frac{3}{2\Delta t}(J^{**} - J^*) = -\frac{\alpha}{\varepsilon}(J^{**} - n^{k+1}u^{k+1}),$$
$$\frac{3}{2\Delta t}(u^{k+1} - u^*) + \nabla_x(p^{k+1} - p^k) = \frac{\alpha}{\varepsilon}\kappa(J^{**} - n^{k+1}u^{k+1}). \tag{28}$$

With J^{**} canceled, one has

$$u^{k+1} + \frac{\frac{3}{2\Delta t} + \frac{\alpha}{\varepsilon}}{\frac{3}{2\Delta t} + \frac{\alpha}{\varepsilon}(1 + \kappa n^{k+1})}\frac{2\Delta t}{3}\nabla_x(p^{k+1} - p^k) = \frac{(\frac{3}{2\Delta t} + \frac{\alpha}{\varepsilon})u^* + \frac{\alpha}{\varepsilon}\kappa J^*}{\frac{3}{2\Delta t} + \frac{\alpha}{\varepsilon}(1 + \kappa n^{k+1})}. \tag{29}$$

Then as in the first order scheme, one can take the divergence of both side. The first term vanishes since u^{k+1} is divergence free. One can solve for $p^{k+1} - p^k$. Then p^{k+1} is derived.

Finally f^{k+1} is solved based on the kinetic Eq. (1),

$$\frac{3f^{k+1} - 4f^k + f^{k-1}}{2\Delta t} + (v \cdot \nabla_x - \nabla_x \Phi \cdot \nabla_v)(2f^k - f^{k-1}) = \frac{1}{\varepsilon}L_{u^{k+1}}f^{k+1}, \tag{30}$$

and J^{k+1} is updated by taking the first moment of f^{k+1}.

Eqs. (25)–(30) give a second order scheme in time. We will check this convergence order numerically in Section 4.1.

Note that this second order scheme is a multistep method. To compute the solutions at t^{k+1}, we need the solutions from both t^k and t^{k-1}. Therefore, with initial data at t^0, it is necessary to apply the first order method to obtain the solutions at t^1. Then this second order scheme can be started.

Remark 3.2. We can formally check the second order accuracy. A rigorous proof is out of the scope of this paper.

First, (26) is (at least) a first order time discretization of the system (8) and (3). The local truncation error gives,

$$u^* = u^{k+1} + O(\Delta t^2), \quad J^* = J^{k+1} + O(\Delta t^2). \tag{31}$$

Next we add up Eqs. (26) and (28):

$$\frac{1}{2\Delta t}(3J^{**} - 4J^k + J^{k-1}) = -\int v \otimes v \nabla_x f^\dagger \mathrm{d}v - n^\dagger \nabla_x \Phi - \frac{1}{\varepsilon}(J^{**} - n^{k+1}u^{k+1}) + R_1,$$
$$\frac{1}{2\Delta t}(3u^{k+1} - 4u^k + u^{k-1}) - \Delta_x u^{k+1} + \nabla_x p^{k+1} = -\nabla_x \cdot (u \otimes u)^\dagger + \frac{1}{\varepsilon}\kappa(J^{**} - n^{k+1}u^{k+1}) + R_2,$$

where the remainder terms are given by

$$R_1 = -\frac{1-\alpha}{\varepsilon}\left((J^* - n^{k+1}u^*) - (J^{**} - n^{k+1}u^{k+1})\right),$$

$$R_2 = \frac{1-\alpha}{\varepsilon}\kappa\left((J^* - n^{k+1}u^*) - (J^{**} - n^{k+1}u^{k+1})\right) + \Delta_x(u^* - u^{k+1}).$$

Noting that (28) combined with (26) is also (at least) a first order time discretization of the system (8) and (3), one has $J^{**} = J^{k+1} + O(\Delta t^2)$. Combined with (31), one has

$$R_1 = O(\Delta t^2), \quad R_2 = O(\Delta t^2).$$

Therefore u^{k+1} and J^{**} are second order approximations of $u(t^{k+1})$ and $J(t^{k+1})$. Then the distribution f^{k+1} is solved via the second order discretization (30).

3.4. The AP property

Now we show that the first order scheme (16), (17a), (17b), (18)–(24) is asymptotic preserving and the limiting scheme gives a first order approximation for the limiting system (10), (11).

As $\varepsilon \to 0$, (24) gives

$$L_{u^{k+1}}f^{k+1} = O(\varepsilon), \quad \text{for } k \geqslant 0.$$

This is equivalent to

$$f^k = n^k M_{u^k} + O(\varepsilon), \quad \text{for } k \geqslant 1.$$

Then one has

$$J^k = n^k u^k + O(\varepsilon),$$

$$\int_{\mathbb{R}^N} v \otimes v f^k \, dv = n^k u^k \otimes u^k + n^k \mathbb{I} + O(\varepsilon).$$

Therefore, (16) is just

$$\frac{1}{\Delta t}(n^{k+1} - n^k) = -\nabla_x \cdot (n^k u^k) + O(\varepsilon). \tag{32}$$

Besides, Eq. (17a) gives

$$J^* = n^{k+1}u^* + O(\varepsilon).$$

Multiply (17a) by κ and add to (17b). One obtains,

$$\frac{1}{\Delta t}\left((1 + \kappa n^{k+1})u^* - (1 + \kappa n^k)u^k\right) - \Delta_x u^* = -\nabla_x \cdot \left((1 + \kappa n^k)u^k \otimes u^k\right) - \kappa \nabla_x n^k - \kappa n^k \nabla_x \Phi + O(\varepsilon). \tag{33}$$

Eq. (32) and (33) give a first order discretization of the limiting system (10), (11), without the pressure term.

Moreover, as $\varepsilon \to 0$, (21) becomes,

$$u^{k+1} + \frac{1}{1 + \kappa n^{k+1}}\Delta t \nabla_x p^{k+1} = u^*, \tag{34}$$

which is exactly the projection step for (10), (11).

Similarly one can show the $\varepsilon \to 0$ limit of (25)–(30) is

$$\frac{1}{2\Delta t}(3n^{k+1} - 4n^k + n^{k-1}) = -\nabla_x \cdot (n^k u^k)^\dagger,$$

$$\frac{1}{2\Delta t}\left(3(1 + \kappa n^{k+1})u^* - 4(1 + \kappa n^k)u^k + (1 + \kappa n^{k-1})u^{k-1}\right) - \Delta_x u^* + \nabla_x p^k = -\nabla_x \cdot ((1 + \kappa n)u \otimes u)^\dagger - \kappa \nabla_x n^\dagger - \kappa n^\dagger \nabla_x \Phi,$$

$$\frac{3(u^{k+1} - u^*)}{2\Delta t} + \frac{1}{1 + \kappa n^{k+1}}\nabla_x(p^{k+1} - p^k) = 0,$$

$$\nabla_x \cdot u^{k+1} = 0. \tag{35}$$

It is the second order projection scheme described in Section 3.1.2 for the limiting system (10), (11), an INS system with spatial variable density $(1 + \kappa n)$.

3.5. Full discretization

3.5.1. Space and velocity discretization

For the sake of concreteness, let us discuss space and velocity discretization issues by restricting to the two-dimension case. The extension to higher dimension is straightforward. Only Cartesian grids are considered. We denote by Δx the (uniform) mesh size. We define a regularly spaced and symmetric velocity grid, with step Δv. Denoting $\mathbf{j} = (j, j')$ and $\mathbf{m} = (m, m')$ in $\mathbb{N}^2$, $f_{\mathbf{j};\mathbf{m}}^k$ stands for the numerical approximation of $f(k\Delta t, (\mathbf{j} - \mathbf{1/2})\Delta x, (\mathbf{m} - \mathbf{1/2})\Delta v - v_{\max})$. Here we assume $v \in [-v_{\max} v_{\max}]^2$. The grid points are located in the cell center.

For the transport term $v \cdot \nabla_x f$ in (24) and (30), we apply the upwind type second order shock capturing schemes (see [36]). Discrete differential operators are defined dimension-by-dimension.

The specular reflection law is used to define the ghost points. For instance, labeling the numerical unknown with indices $j, j' \in \{1, \ldots, J\}$ and $m, m' \in \{1, \ldots, 2M\}$, where the M first (resp. last) velocities are negative (resp. positive), leads to

$$f_{0,j';m,m'}^k = f_{1,j';2M+1-m;m'}^k, \quad f_{J+1,j';m,m'}^k = f_{J,j';2M+1-m,m'}^k.$$

For the pressure, Neumann boundary condition (22) leads to

$$p_{0,j'}^{k+1} = p_{1,j'}^{k+1}, \quad p_{J+1,j'}^{k+1} = p_{J,j'}^{k+1}.$$

The no-slip boundary of u^* (19) leads to
$$u_{0,j'}^* = -u_{1,j'}^*, \quad u_{J+1,j'}^* = -u_{J,j'}^*.$$

Similar expression holds when exchanging the role of u_1^*, u_2^*, j, j' and m', m'.

The convection term $\nabla_x \cdot (u \otimes u)$ and the diffusion term $\Delta_x u$ in incompressible Navier–Stokes system (3), as well as the terms $\nabla_x \cdot u^*$ and $\nabla_x p$ in the projection steps (22) – (21), are approximated by centered differences.

Macroscopic quantities are defined by using the 2-dimensional version of the trapezoidal rule in order to ensure that the even moments of the odd functions with respect to v vanish.

The derivative with respect to velocity which appears in the acceleration term is also solved by the upwind type second order shock capturing schemes (see [36]).

3.5.2. Inversion of the Fokker–Planck operator

We have already discussed the discretization of the transport term. Now we focus on how to solve f^{k+1} from (24), where the stiff term is treated implicitly. We need to invert the Fokker–Planck operator. To this end, we follow the approach introduced in [39]. We write

$$L_u f = \sqrt{M_u} \tilde{L}_u h$$

with

$$h = \frac{f}{\sqrt{M_u}}, \quad \tilde{L}_u h = \frac{1}{\sqrt{M_u}} \nabla_v \cdot \left(M_u \nabla_v \left(\frac{h}{\sqrt{M_u}} \right) \right).$$

Note that $\tilde{L}_u$ is symmetric for the standard L^2 inner product

$$\int_{\mathbb{R}^N} \tilde{L}_u h \, g \, dv = \int_{\mathbb{R}^N} h \, \tilde{L}_u g \, dv.$$

Accordingly, we set

$$h_{\mathbf{j};\mathbf{m}} = \frac{f_{\mathbf{j};\mathbf{m}}^{k+1}}{\sqrt{M_{\mathbf{j};\mathbf{m}}^{k+1}}}, \quad \mathscr{L} f_{\mathbf{j};\mathbf{m}}^{k+1} = \sqrt{M_{\mathbf{j};\mathbf{m}}^{k+1}} \, \tilde{\mathscr{L}} h_{\mathbf{j};\mathbf{m}}.$$

The discrete operator $\tilde{\mathscr{L}}$ is symmetric which allows to make use of the Conjugate Gradient algorithm. In dimension two, the discrete operator $\tilde{\mathscr{L}}$ is defined as follows

$$\tilde{\mathscr{L}} h_{j,j';m,m'} = \frac{1}{\Delta v^2} \left(h_{j,j';m,m'+1} + h_{j,j';m+1,m} - \overline{M}_{j,j';m,m'}^{k+1} h_{j,j';m,m'} + h_{j,j';m,m'-1} + h_{j,j';m-1,m'} \right),$$

$$\overline{M}_{j,j';m,m'}^{k+1} = \frac{\sqrt{M_{j,j';m+1,m'}^{k+1}} + \sqrt{M_{j,j';m,m'+1}^{k+1}} + \sqrt{M_{j,j';m-1,m'}^{k+1}} + \sqrt{M_{j,j';m,m'-1}^{k+1}}}{\sqrt{M_{j,j';m,m'}^{k+1}}} \tag{36}$$

which indeed leads to a symmetric matrix. Observe that $\tilde{\mathscr{L}} \left(\sqrt{M^{k+1}} \right)_{\mathbf{j};\mathbf{m}} = 0$. Therefore, the updating of the particles distribution function

$$\left(1 - \frac{\Delta t}{\varepsilon} \mathscr{L} \right) f_{\mathbf{j};\mathbf{m}}^{k+1} = S_{\mathbf{j};\mathbf{m}}^k$$

obeys the following rules:

- Solve the linear system

$$\left(1 - \frac{\Delta t}{\varepsilon}\tilde{\mathscr{L}}\right)h_{\mathbf{j};\mathbf{m}} = \frac{S_{\mathbf{j};\mathbf{m}}^k}{\sqrt{M_{\mathbf{j};\mathbf{m}}^{k+1}}}.$$

- Set $f_{\mathbf{j};\mathbf{m}}^{k+1} = h_{\mathbf{j};\mathbf{m}}\sqrt{M_{\mathbf{j};\mathbf{m}}^{k+1}}$.

4. Numerical simulations

From now on we will use the following notations: $\mathbf{x} = (x,y)$ is the position variable, $\mathbf{v} = (v_1, v_2)$ is the velocity variable, $\mathbf{u} = (u_1, u_2)$ is the fluid velocity and $\mathbf{u}_p = (u_{p1}, u_{p2})$ is the macroscopic particle velocity.

We apply the second order method described in Section 3.3. Unless otherwise specified, we always use the following settings.

The computation is performed on $(\mathbf{x}, \mathbf{v}) \in [0,1]^2 \times [-v_{\max}, v_{\max}]^2$, with $v_{\max} = 8$. The specular boundary condition is applied on particle distribution f, while no-flip boundary condition is used for fluid velocity $\mathbf{u}$.

We take $N_x = 128$ grid points in each x direction and $N_v = 32$ grid points in each v direction. We apply the van Leer type slope limiter on the discretization of the advection parts, and take $\Delta t = \frac{\Delta x}{5 v_{\max}}$, which guarantees the stability.

All the simulations are performed on a PC with a single-core 2.2 GH CPU. Using the second order method with the given numerical parameters, it takes around 6 h to simulate up to time $t = 1$.

We always take

$$f(0, \mathbf{x}, \mathbf{v}) = n(0, \mathbf{x})M_{\mathbf{u}_p(0, \mathbf{x})}$$

as the initial data for particles distribution. Here $\mathbf{u}_p = \frac{J}{n}$ is the macroscopic velocity of particles. Note that this is not necessarily the equilibrium in the sense that $L_{\mathbf{u}}f \neq 0$ in (2) since we do not require $\mathbf{u}_p = \mathbf{u}$.

We take $\kappa = 2$ throughout the simulations. However the schemes can be applied to the case when κ is very large, without any difficulty.

4.1. Convergence order

First we numerically check that the scheme described in Section 3.3 is indeed second order in Δx (therefore in Δt). We start with the initial data

$$n(0, \mathbf{x}) = 10^{-10} + \exp\left(-80(x - 0.5)^2 - 80(y - 0.5)^2\right),$$

$$\mathbf{u}_p(0, \mathbf{x}) = \begin{pmatrix} \sin^2(\pi x)\sin(2\pi y) \\ -\sin^2(\pi y)\sin(2\pi x) \end{pmatrix}, \tag{37}$$

$$\mathbf{u}(0, \mathbf{x}) = \mathbf{u}_p(0, \mathbf{x}).$$

We compute the solutions on a grid of $N_x \times N_x \times N_v \times N_v$, with $N_x = 16, 32, 64, 128$ respectively. As mentioned before, $N_v = 32$. After time $t_{\max} = 0.025$ we check the following error,

$$e_{\Delta x}(f) = \max_{t \in (0, t_{\max})} \frac{\|f_{\Delta x}(t) - f_{2\Delta x}(t)\|_p}{\|f_{2\Delta x}(0)\|_p},$$

$$e_{\Delta x}(\mathbf{u}) = \max_{t \in (0, t_{\max})} \frac{\|\mathbf{u}_{\Delta x}(t) - \mathbf{u}_{2\Delta x}(t)\|_p}{\|\mathbf{u}_{2\Delta x}(t_{\max})\|_p}. \tag{38}$$

This can be considered as an estimation of the relative error in l^p norm, where $f_{\Delta x}$ and $\mathbf{u}_{\Delta x}$ are the numerical solutions computed from a grid of size $\Delta x = \frac{1}{N_x}$. The numerical scheme is said to be k-th order if $e_{\Delta x} \leqslant C\Delta x^k$, for Δx small enough.

Fig. 1 gives the convergence order in l^1 norm for particle distribution f and in l^2 norm for fluid velocity $\mathbf{u}$. This shows that the scheme is second order in space (hence in time) uniformly in ε for both particle distribution f and fluid velocity $\mathbf{u}$, as expected. Here we have turned off the limiters on the convection part to avoid its influence. With the limiters on, the uniform convergence order would be around 1.7.

4.2. AP property

Now we check the AP property we proposed in Section 3.4. We take the volcano like initial data

$$n(0, \mathbf{x}) = (0.5 + 100((x - 0.5)^2 + (y - 0.5)^2))\exp\left(-40(x - 0.5)^2 - 40(y - 0.5)^2\right),$$

$$\mathbf{u}_p(0, \mathbf{x}) = \begin{pmatrix} -\sin(2\pi(y - 0.5)) \\ \sin(2\pi(x - 0.5)) \end{pmatrix}\exp\left(-20(x - 0.5)^2 - 20(y - 0.5)^2\right), \tag{39}$$

$$\mathbf{u}(0, \mathbf{x}) = 0.$$

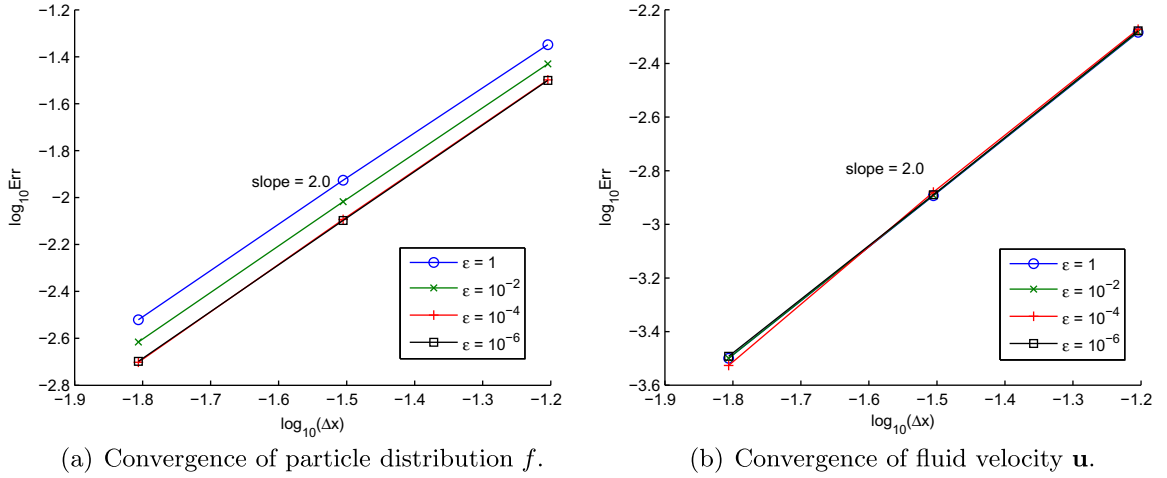(a) Convergence of particle distribution f.   (b) Convergence of fluid velocity $\mathbf{u}$.

Fig. 1. The test of convergence order with initial data (37). This figure shows the l^1 errors (38) in particle distribution f (left) and l^2 norm of fluid velocity $\mathbf{u}$ (right) with different ε.
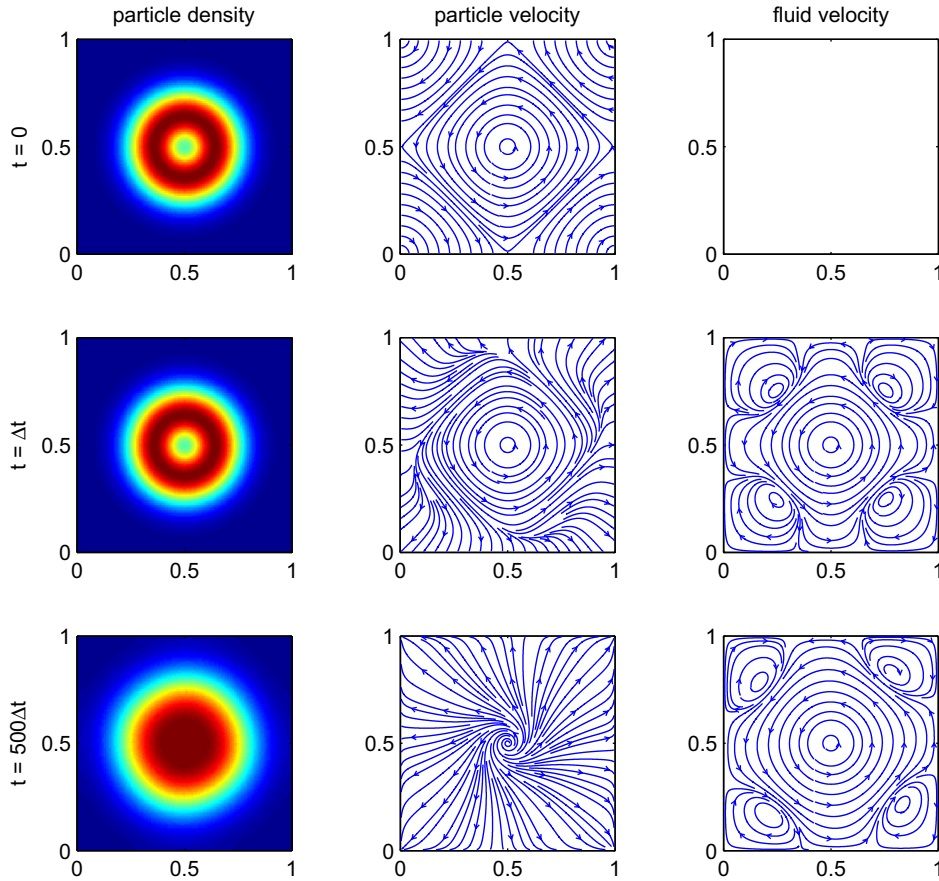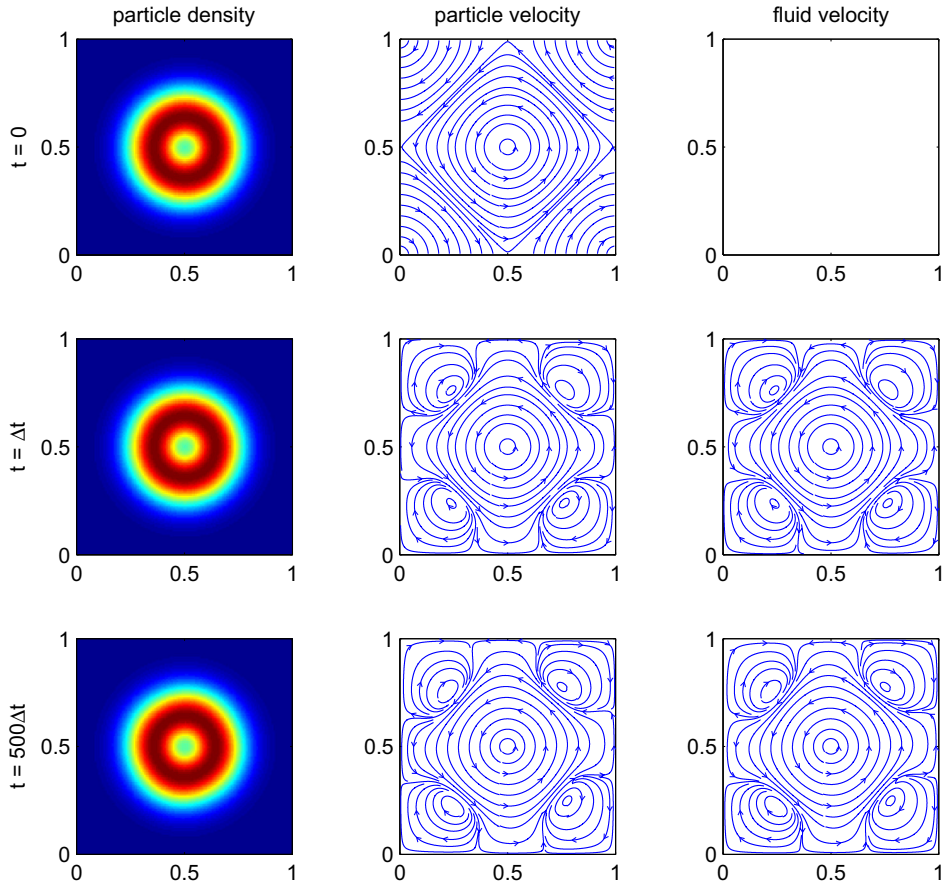

Fig. 2. Numerical simulation with initial data (39) for $\varepsilon = 1$. This figure shows the particle density n (left column), streamlines of particle velocity $\mathbf{u}_p$ (middle column) and fluid velocity $\mathbf{u}$ (right column) at $t = 0$ (upper row), $t = \Delta t$ (middle row) and $t = 500\Delta t$ (lower row). The gravity is neglected.

Fig. 3. Numerical simulation with initial data (39) for $\varepsilon = 10^{-8}$. This figure shows the particle density n (left column), streamlines of particle velocity $\mathbf{u}_p$ (middle column) and fluid velocity $\mathbf{u}$ (right column) at $t = 0$ (upper row), $t = \Delta t$ (middle row) and $t = 500\Delta t$ (lower row). The gravity is neglected.
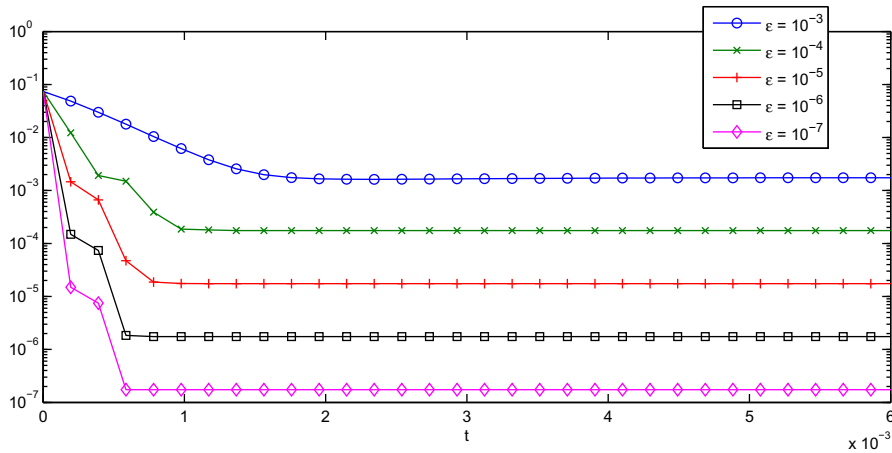
Fig. 4. The time evolution of $\|f - nM_{\mathbf{u}}\|_1$ with different ε, starting with the initial data (39).

Therefore initially $\mathbf{u}_p \neq \mathbf{u}$ and the equilibrium is not assumed. We apply the second order scheme and perform the simulation until $t_{\max} = 0.5$. In Fig. 2, where $\varepsilon = 1$, we show the pictures of particle density n, streamlines of particle velocity $\mathbf{u}_p$ and fluid velocity $\mathbf{u}$ at t^0 (the initial time), t^1 (after one time step) and t^{450} (the end time). The streamlines of particles and fluid are totally different. The particles expand to the whole square domain and are not significantly affected by the circulating fluid. We show the same quantities in Fig. 3 with $\varepsilon = 10^{-5}$. In this case the drag force between different phases is so strong
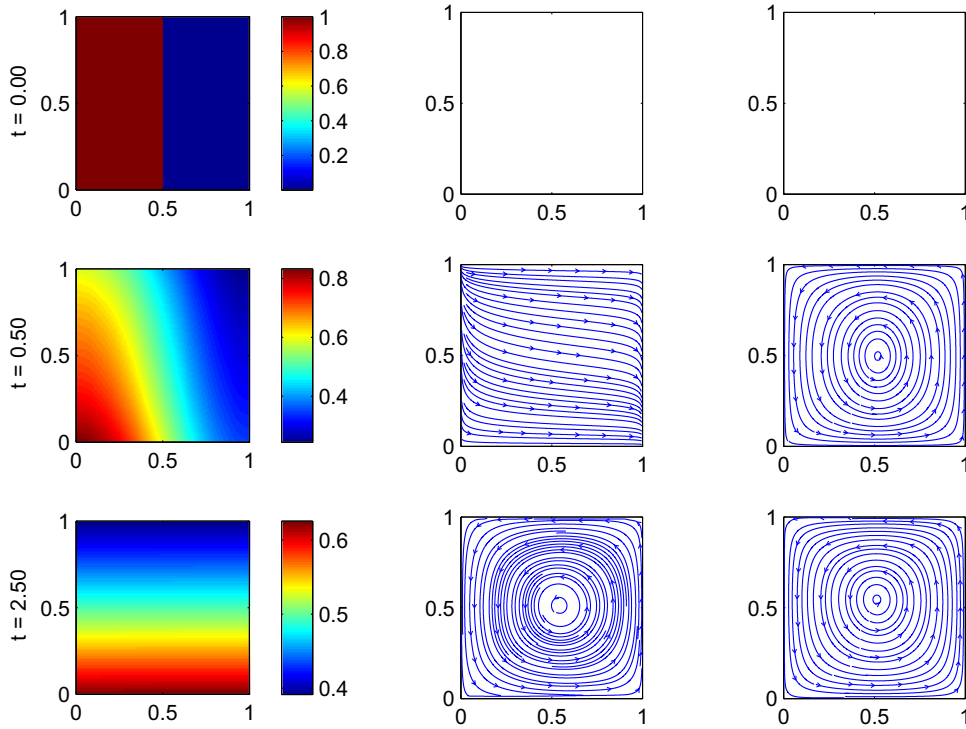
Fig. 5. The time evolution of particle density (left) and streamlines of velocities of particles (middle) and fluid (right) corresponding to the dam like initial data. The gravity is considered. $\varepsilon = 1$.

that the particles also circulate in the square domain. Besides, the expansion in particle density is decelerated by the fluid. The particles keep the volcano shape well in this period of time.

At last, we check the time evolution of l^1 distances $\|f - nM_{\mathbf{u}}\|_1$. Note that $M_{\mathbf{u}}$ is a Maxwellian centered at the fluid velocity **u**. The result is shown in Fig. 4. As expected, we have $f - nM_{\mathbf{u}} = O(\varepsilon)$ after one time step. This gives a direct evidence of the AP property we proposed.

4.3. Some applications

Our schemes are easily extended to more complicated circumstances. In this section we apply our schemes to several different problems. We also incorporate the Reynolds number into the incompressible Navier–Stokes system in the usual way

$$\begin{cases} \partial_t u + \nabla_x \cdot (u \otimes u) + \nabla_x p - \frac{1}{\mathrm{Re}} \Delta_x u = \frac{1}{\varepsilon} \kappa \int (v - u) f \, \mathrm{d}v, \\ \nabla_x \cdot u = 0. \end{cases} \tag{40}$$

The parameters in our simulation allow us to compute with Reynolds number up to $\mathrm{Re} = 1000$ without trouble in stability. In the following simulation we will take $\mathrm{Re} = 1000$. Larger Reynolds number, which requires smaller mesh size Δx for the sake of accuracy, is beyond the scope of this work.

In Section 4.3.1 the external force (the gravity) is considered. In Section 4.3.2 a different boundary condition is applied to the particle distribution f, while in Section 4.3.3 we apply a different boundary condition to the fluid velocity **u**.

4.3.1. Simulation of gravity driven flow

Now we consider the dam like initial data,

$$n(0, \mathbf{x}) = 10^{-10} + \mathbf{1}_{0 \leqslant x \leqslant 0.5},$$
$$\mathbf{u}_p(0, \mathbf{x}) = 0, \tag{41}$$
$$\mathbf{u}(0, \mathbf{x}) = 0.$$

In this case the movement of particles and fluid are initiated by the gravity. We include the external force term $\nabla_x \Phi \cdot \nabla_v f$ in our simulation, where $\Phi = gy$ with gravity constant $g = 1$. The particles are uniformly distributed on the left hand side. As the simulation starts, the particles fall down and cause the circulation of fluid.

Fig. 5 shows the time evolution of particle density (left) when $\varepsilon = 1$, as well as the evolution of streamlines of velocity of particles (middle) and fluid (right). In this case the drag force between particles and fluid is not significant. The particles just

fall down and cover the whole bottom. The streamlines show clearly the behavior of particles is quite different from that of the fluid.

Fig. 6 shows the time evolution of particle density when $\varepsilon = 10^{-3}$. Now the drag force between particles and fluid is stronger. The streamlines of particles and the fluid are similar all the time. As time evolves, the particles fall down and drive the fluid to circulate counter-clockwisely. Then the particles follow this circulation. Finally the particles settle at the bottom uniformly due to the loss of energy.

Fig. 7 shows the time evolution of particle density when $\varepsilon = 10^{-8}$. In this case the drag force between particles and fluid is so strong that the particles and the fluid always keep the same pace. The solution behavior is quite similar to the case when $\varepsilon = 10^{-3}$. But it has a much smaller dissipation effect in the particle density. In fact, since ε is quite small, the composite density $(1 + \kappa n)$ satisfies the INS system (10), (11). The only diffusion effect in particle density is due to the numerical dissipation.

We also solve the limiting composite incompressible Navier–Stokes system with variable density (10), (11) directly by the second order method in Section 3.1.2, with the same initial data (41). The numerical result at time $t = 5$ is shown in Fig. 8 (right). To compare, the composite density $(1 + \kappa n)$ obtained from the kinetic system (1)–(3) with different ε is also shown in Fig. 8. As $\varepsilon \to 0$, the solution to the kinetic system approaches to that of the limiting system, which shows that the AP property is obtained.

4.3.2. Simulation of Injecting Problem

Now let us consider the situation when the particles are injected into the square domain. We take the initial data as follows.
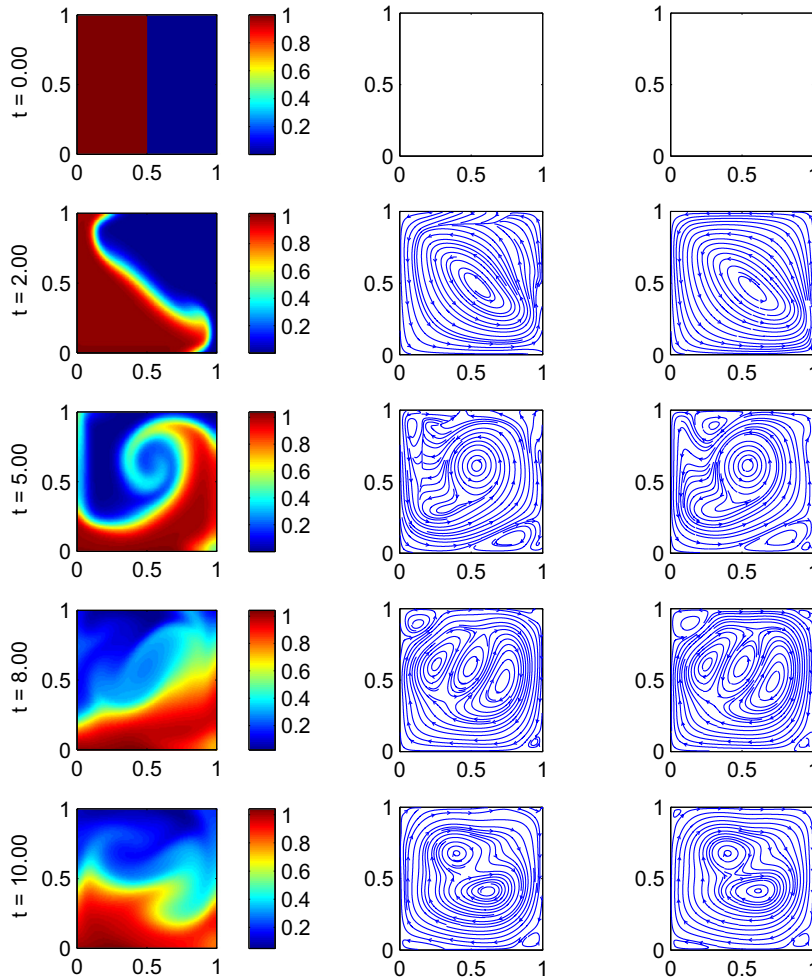

Fig. 6. The time evolution of particle density (left) and streamlines of velocities of particles (middle) and fluid (right) corresponding to the dam like initial data. The gravity is considered. $\varepsilon = 10^{-3}$.
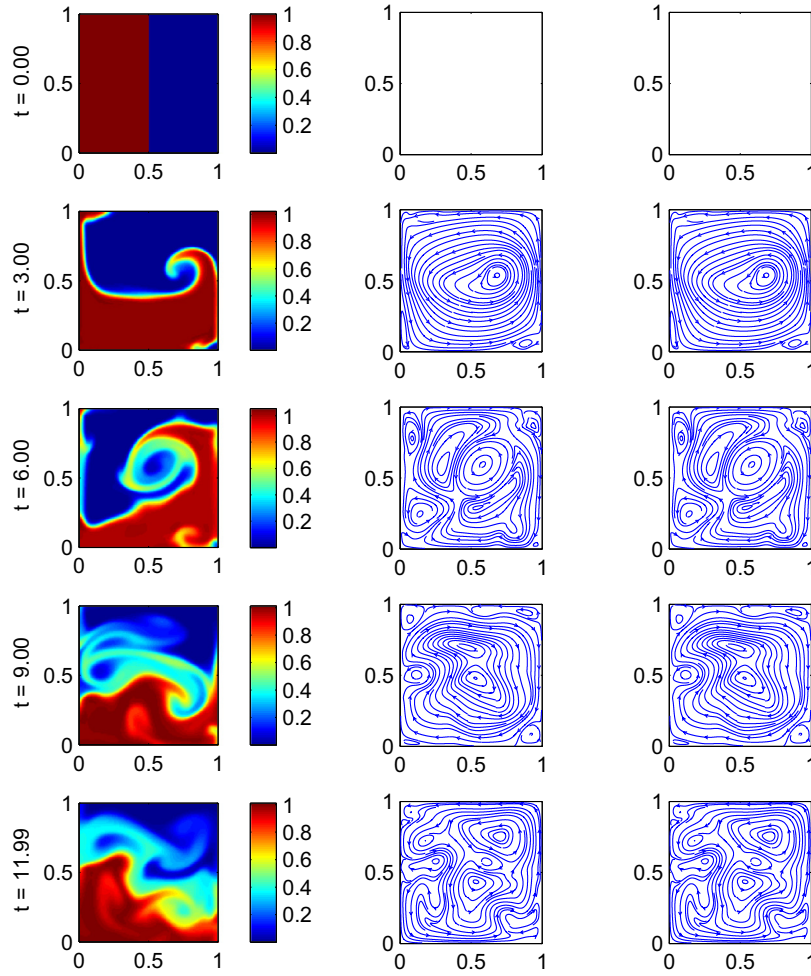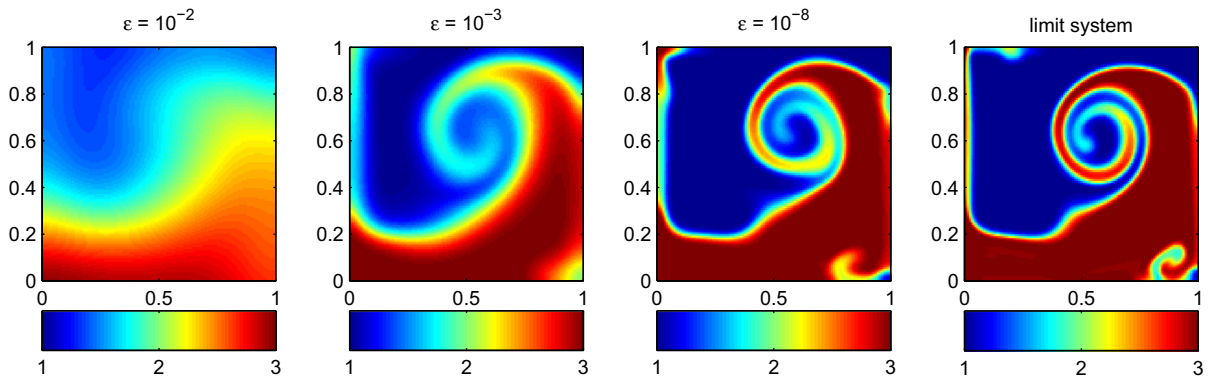
Fig. 7. The time evolution of particle density (left) and streamlines of velocities of particles (middle) and fluid (right) corresponding to the dam like initial data. The gravity is considered. $\varepsilon = 10^{-8}$.

Fig. 8. The composite density $(1 + \kappa n)$ at time $t = 5$ for different systems with the dam like initial data (41). From left to right, kinetic system (1)–(3) with $\varepsilon = 10^{-2}, \varepsilon = 10^{-3}, \varepsilon = 10^{-8}$ and the limiting Navier–Stokes systems (10) and (11).

$$n(0, \mathbf{x}) = 10^{-10}, \quad \mathbf{u}_p(0, \mathbf{x}) = \mathbf{u}(0, \mathbf{x}) = 0.$$

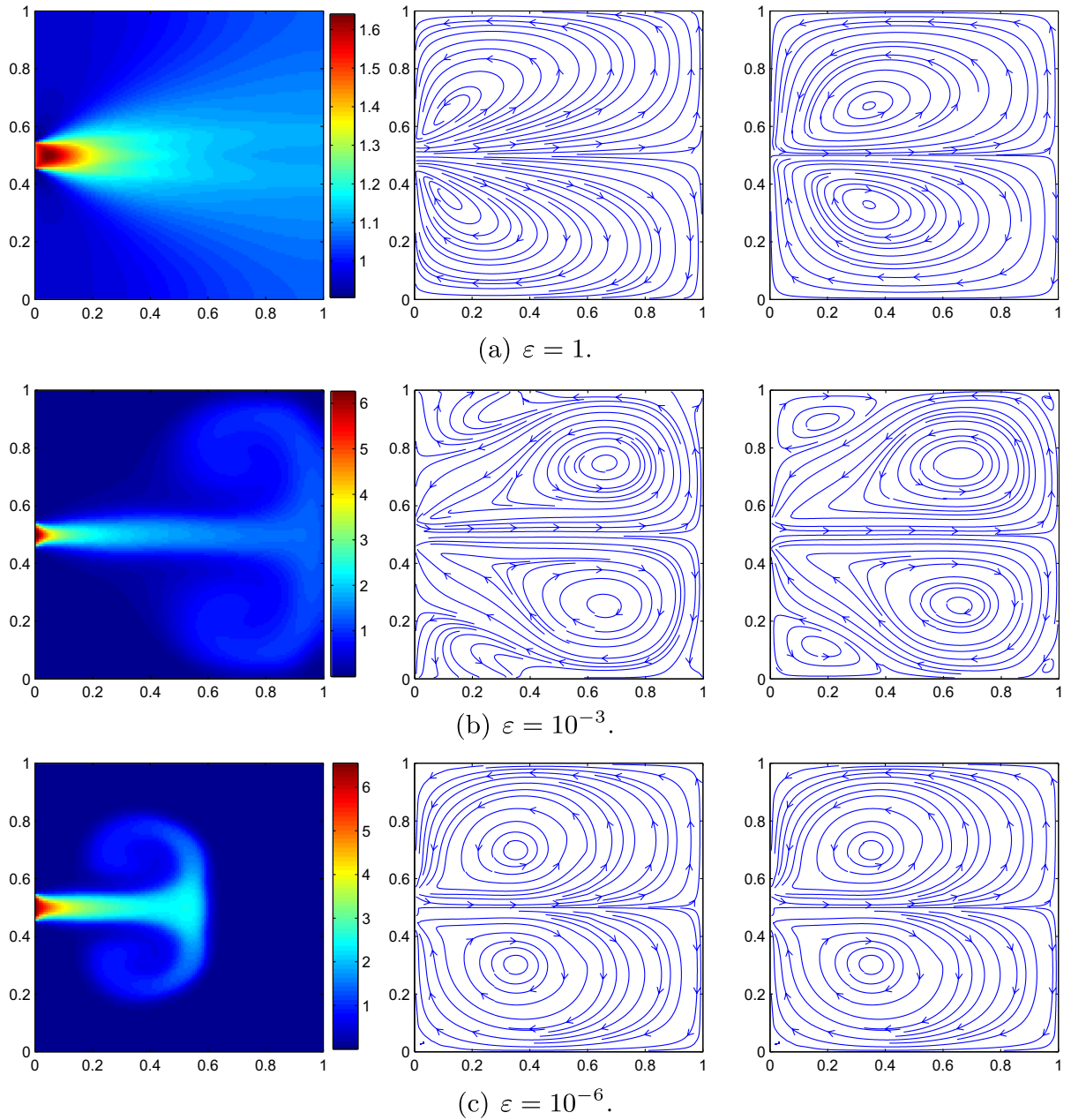The injecting particle flow is described by the boundary condition on f,

Fig. 9. The particle density (left), streamlines of velocities of particles (middle) and fluid (right) at $t = 5$ for the injecting problem, with different ε. The gravity is neglected.

$$f(t, \mathbf{x}, \mathbf{v}) = 1_{2 \leqslant v_1 \leqslant 3}, \quad \text{if } \mathbf{x} \in \Gamma$$

where v_1 is the first component of $\mathbf{v}$. The entrance of flow Γ locates at the center of the left boundary,

$$\Gamma = \{(0, y) | 0.45 \leqslant y \leqslant 0.55\}.$$

We perform the simulation with different ε. In Fig. 9 we show the particle density (left) and streamlines of particle velocity (middle) and fluid velocity (right) at time $t = 5$. We ignore the gravity effect.

In Fig. 9(a), where $\varepsilon = 1$, the particles spread to the right end of the domain. The streamlines of fluid and particles are quite different, which suggests the interaction between them are not obvious.

In Fig. 9(b), where $\varepsilon = 10^{-3}$, the spreading of particles to the right end is decelerated by the strong drag force from the fluid. A mushroom-shape front is formed. The streamline of particles and fluid are similar to each other, with visible difference.
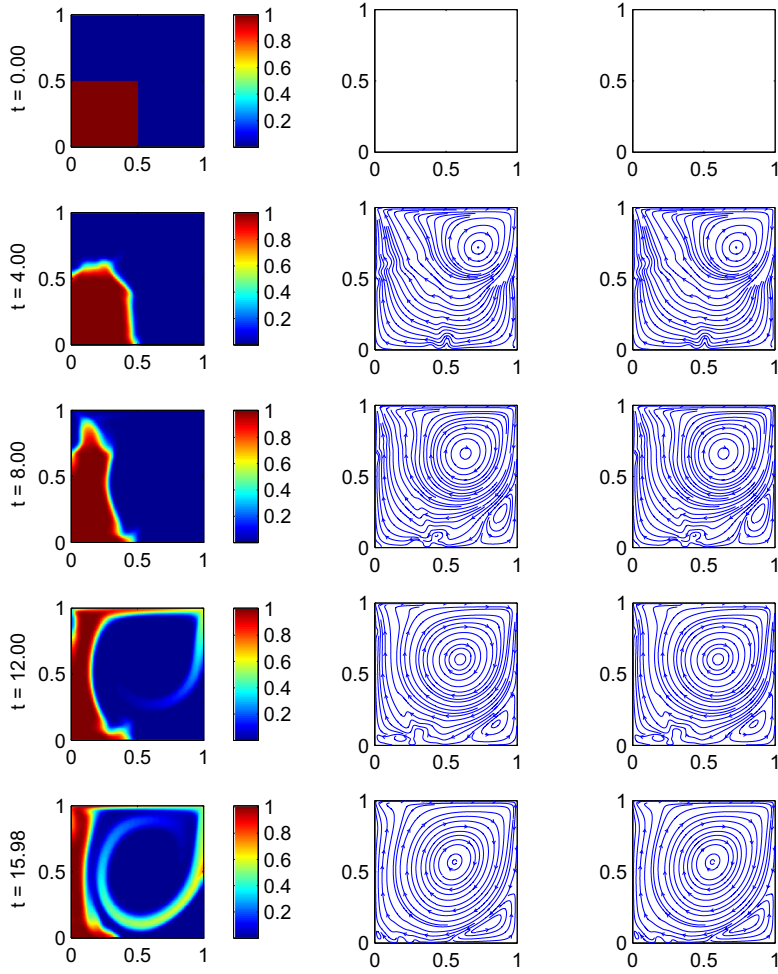
Fig. 10. The time evolution of cavity flow, with Reynolds number Re = 1000. Here $\varepsilon = 10^{-8}$. The gravity is neglected. Left: the particle density; Middle: streamlines of velocities of particles (middle); Right: streamlines of velocities of fluid (right).
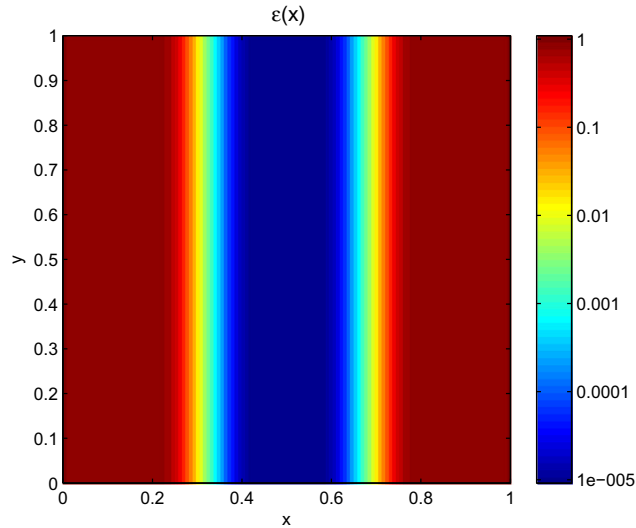

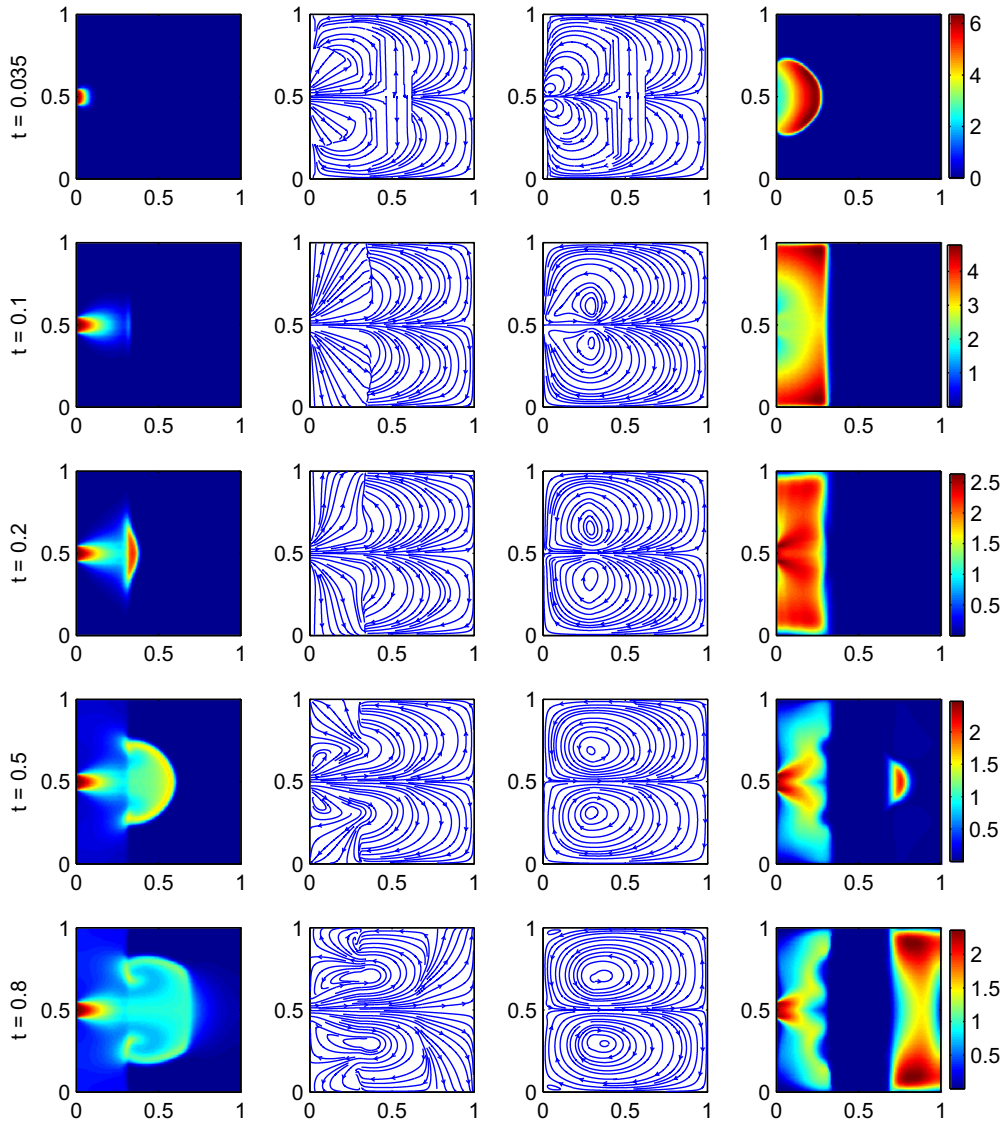**Fig. 11.** The x-dependent function $\varepsilon(x)$ given by (42), with $\varepsilon_0 = 10^{-5}$.

Fig. 12. The time evolution of injecting problem in mixing regime. From left to right are the particle density, the particle velocity $\mathbf{u}_p$, the fluid velocity $\mathbf{u}$ and $|\mathbf{u}_p - \mathbf{u}|$.

In Fig. 9(c), where $\varepsilon = 10^{-6}$, a similar mushroom-shape front is formed, with a lower spreading speed. The streamline of particles and fluid are quite close to each other.

4.3.3. Simulation of cavity flow

Finally we apply our scheme to cavity flow. The cavity flow happens in a wide range of area, for example, the car sunroof and aircraft landing gear well.

We simulate the fluid flowing past an open cavity. Initially the cavity is full of rest fluid and the particle sediments are resting near the bottom corner of the cavity. The outside fluid flows past the opening of the cavity with a constant velocity, which drives the inside fluid circulating in the cavity. For simplicity we assume that the particle cannot escape the cavity, although our scheme can be easily generalized to the case when this escape happens.

We give the initial and boundary conditions corresponding to this description,

$$n(0, \mathbf{x}) = 10^{-10} + \mathbf{1}_{0 \leqslant x \leqslant 0.5, 0 \leqslant y \leqslant 0.5},$$
$$\mathbf{u}_p(0, \mathbf{x}) = 0,$$
$$\mathbf{u}(0, \mathbf{x}) = 0.$$

with

$$\mathbf{u}(t, \mathbf{x}) = \begin{pmatrix} 1 \\ 0 \end{pmatrix}, \quad \text{if } y = 1.$$

We need to modify (19) accordingly to incorporate this boundary condition.

We take $\varepsilon = 10^{-8}$ and neglect the gravity effect. The simulation is performed with Reynolds number Re = 1000. Fig. 10 (left) shows the time evolution of particle density distribution until $t_{\max} = 16$. The particles move along the streamline of fluid and circulate in the cavity. A second circulation is observed in the right corner.

4.3.4. Simulation of injection problem in mixing regime

Until now we have considered the case that ε is a constant over the spatial domain. However one of the advantages of AP schemes is that they can capture the solution behaviors in different regimes automatically. Illustrated by [45], we study a mixing regime problem, with an **x**-dependent $\varepsilon(\mathbf{x})$,

$$\varepsilon(x, y) = 1 + \varepsilon_0 - \frac{1}{2}(\tanh(10 - 40(x - 0.5)) + \tanh(10 + 40(x - 0.5))). \tag{42}$$

We take $\varepsilon_0 = 10^{-5}$. $\varepsilon(\mathbf{x})$ varies from ε_0 to $O(1)$ smoothly, as shown in Fig. 11.

We study the injecting problem in the mixing regime. We take exactly the same physical and numerical parameters as in Section 4.3.2, except $\varepsilon(\mathbf{x})$. We do not discuss here the physical relevancy of working with space variable ε's; we only discuss (42) as an evidence of feasibility.

From left to right, Fig. 12 shows several snapshots of the time evolution of the particle density, the particle velocity, the fluid velocity and the discrepancy of the two velocities $|\mathbf{u}_p - \mathbf{u}|$. The two phases behave quite differently in the weak interaction regimes where $\varepsilon = O(1)$. While in the strong interaction regime ($\varepsilon \ll 1$), $|\mathbf{u}_p - \mathbf{u}| \ll 1$, which suggests that the fluid limit of this two-phase system is achieved automatically in this domain.

References

[1] M. Ishii, T. Hibiki, Thermo-Fluid Dynamics of Two-Phase Flows, Springer, New York, NY, USA, second edition.
[2] P.J. O'Rourke, Collective drop effects on vaporizing liquid sprays, Ph.D. thesis, Princeton Univ., available as Technical Report #87545 Los Alamos National Laboratory (1981).
[3] C. Baranger, G. Baudin, L. Boudin, B. Després, F. Lagoutière, F. Lapébie, T. Takahashi, Liquid jet generation and break-up, in: S. Cordier, T. Goudon, M. Gutnic, E. Sonnendrucker (Eds.), Numerical methods for hyperbolic and kinetic equations, IRMA Lectures in Mathematics and Theoretical Physics, vol. 7, EMS Publ. House, 2005.
[4] C. Baranger, L. Boudin, P.-E. Jabin, S. Mancini, A modeling of biospray for the upper airways, ESAIM:Proc. 14 (2005) 41–47.
[5] L. Desvillettes, Some new results of existence for the theory of sprays, <http://www.newton.ac.uk/programmes/KIT/seminars/090710001.html>, workshop Fluid-Kinetic Modeling in Biology, Physics and Engineering, Isaac Newton Institute for Mathematical Sciences, Programme on PDEs in Kinetic Theories (2010)
[6] A. Moussa, Etude mathématique et numérique du transport d'aérosols dans le poumon humain, Ph.D. thesis, ENS Cachan (2009).
[7] S. Berres, R. Bürger, E.M. Tory, Mathematical model and numerical simulation of the liquid fluidization of polydisperse solid particle mixtures, Comput. Vision Sci. 6 (2004) 67–74.
[8] Y. Sina, P. Stopford, M. Edwards, S. Watkins, CFD modeling of fire suppression by water spray: sensitivity and validation for a pool fire in a room, in: Eighth International IBPSA Conference Eindhoven, Netherlands, 2003.
[9] B. Sportisse, Modélisation et simulation de la pollution atmosphérique, Ph.D. thesis, Université Pierre et Marie Curie, habilitation à Diriger les Recherches, Sciences de l'Univers (2007).
[10] I. Vinkovic, Dispersion et mélange turbulents de particules solides et de gouttelettes par une simulation des grandes échelles et une modélisation stochastique lagrangienne. application à la pollution de l'atmosphère, Ph.D. thesis, Ecole Centrale de Lyon (2005).
[11] M. De Luca, Contribution à la modélisation de la pulvérisation d'un liquide phytosanitaire en vue de réduire les pollutions, Ph.D. thesis, Univ. Aix-Marseille 2 (2007).
[12] N.A. Patankar, D.D. Joseph, Modeling and numerical simulation of particulate flows by the Eulerian–Lagrangian approach, Int. J. Multiphase Flow 27 (2001) 1659–1684.
[13] N.A. Patankar, D.D. Joseph, Lagrangian numerical simulation of particulate flows, Int. J. Multiphase Flow 27 (2001) 1685–1706.
[14] D.M. Snider, P.J. O'Rourke, M.J. Andrews, Sediment flow in inclined vessels calculated using a multiphase particle-in-cell model for dense particle flows, Int. J. Multiphase Flow 24 (1998) 1359–1382.
[15] J. Mathiaud, Etude de systèmes de type gaz-particules, Ph.D. thesis, ENS Cachan (2006).
[16] F.A. Williams, Combustion Theory, second ed., Benjamin Cummings Publ., 1985.
[17] G. Lavergne, Modélisation de l'écoulement multiphasique dans le propulseur à poudre P230 d'Ariane 5, lecture Notes of the School of the Groupement Français de Combustion, Ile d'Oléron (2004).
[18] A. Einstein, Eine neue bestimmung der moleküldimensionen, Ann. Physik 19 (1906) pp. 289–306, doctoral dissertation, Zürich, 1905.
[19] A. Einstein, On the motion of small particles suspended in liquids at rest required by the molecular-kinetic theory of heat, Ann. Physik 17 (1905) 549–560.

[20] L. Desvillettes, F. Golse, V. Ricci, The mean-field limit for solid particles in a Navier–Stokes flow, J. Stat. Phys. 131 (5) (2008) 941–967, http://dx.doi.org/10.1007/s10955-008-9521-3.
[21] V.S. Galkin, S.V. Rusakov, Kinetic Fokker–Planck equation for free-molecular, thermally nonequilibrium Brownian particles in an inhomogeneous gas, Fluid Dynamics 42 (2007) pp. 330–334, originally published in Izvestiya Rossiiskoi Akademii Nauk, Mekhanika Zhidkosti i Gaza 42 (2) (2007) pp. 204–208 (in Russian).
[22] R. Caflisch, G. Papanicolaou, Dynamic theory of suspensions with Brownian effects, SIAM J. Appl. Math. 43 (1983) 885–906.
[23] J.A. Carrillo, T. Goudon, Stability and asymptotics analysis of a fluid-particles interaction model, Commun. PDE 31 (2006) 1349–1379.
[24] K. Hamdache, Global existence and large time behavior of solutions for the Vlasov–Stokes equations, Jpn J. Ind. Appl. Math. 15 (1998) 51–74.
[25] L. Boudin, L. Desvillettes, C. Grandmont, A. Moussa, Global existence of solutions for the coupled Vlasov and Navier–Stokes equations, Differ. Integral Equ., vol. 22 pp. 11–12.
[26] A. Mellet, A. Vasseur, Global weak solutions for a Vlasov–Fokker–Planck/Navier–Stokes system of equations, Math. Mod. Meth. Appl. Sci 17 (7) (2007) 1039–1063.
[27] T. Goudon, A. Moussa, L. He, P. Zhang, The Navier–Stokes–Vlasov–Fokker–Planck system near equilibrium, SIAM J. Math. Anal. 42 (5) (2010) 2177–2202.
[28] J.A. Carrillo, K. Karpery, K. Trivisa, On the dynamics of a fluid-particle interaction model: the bubbling regime, Nonlinear Anal. TMA 74 (2011) 2778–2801.
[29] T. Goudon, P.-E. Jabin, A. Vasseur, Hydrodynamic limit for the Vlasov–Navier–Stokes equations. II. Fine particles regime, Indiana Univ. Math. J. 53 (6) (2004) 1517–1536.
[30] A. Mellet, A. Vasseur, Asymptotic analysis for a Vlasov–Fokker–Planck/compressible Navier–Stokes system of equations, Commun. Math. Phys. 281 (3) (2008) 573–596.
[31] C. Baranger, L. Desvillettes, Coupling Euler and Vlasov equations in the context of sprays: local smooth solutions, J. Hyper. Differ. Equ. 3 (1) (2006) 1–26.
[32] J.A. Carrillo, T. Goudon, P. Lafitte, Simulation of fluid & particles flows: asymptotic preserving schemes for bubbling and flowing regimes, J. Comput. Phys. 227 (16) (2008) 7929–7951.
[33] J.A. Carrillo, R. Duan, A. Moussa, Global classical solutions close to equilibrium to the Vlasov–Euler–Fokker–Planck system, Kinet. Relat. Models 4 (1) (2011) 227–258.
[34] L. Boudin, B. Boutin, B. Fornet, T. Goudon, P. Lafitte, F. Lagoutière, B. Merlet, Fluid-particles flows: a thin spray model with energy exchanges, ESAIM: Proc. 28 (2009) 195–210.
[35] B. Boutin, P. Lafitte, Splitting schemes for fluid-particles flows with energy exchanges, work in progress.
[36] T. Goudon, S. Jin, B. Yan, Simulation of fluid-particles flows: Heavy particles, flowing regime and AP-schemes, Commun. Math. Sci. 10 (2012) 355–385.
[37] S. Jin, Efficient asymptotic-preserving (AP) schemes for some multiscale kinetic equations, SIAM J. Sci. Comput. 21 (2) (1999) 441–454.
[38] S. Jin, Asymptotic preserving (AP) schemes for multiscale kinetic and hyperbolic equations: a review., Lecture Notes for Summer School on Methods and Models of Kinetic Theory (M&MKT), Porto Ercole (Grosseto, Italy), June 2010. Rivista di Matematica della Universita di Parma 3 (2012) pp. 177–216.
[39] S. Jin, B. Yan, A class of asymptotic-preserving schemes for the Fokker–Planck–Landau equation, J. Comput. Phys. 230 (17) (2011) 6420–6437, http://dx.doi.org/10.1016/j.jcp.2011.04.002.
[40] A. Chorin, The numerical solution of the Navier-Stokes equations for an incompressible fluid, Bull. Am. Math. Soc. 73 (1967) 928–931.
[41] A. Chorin, On the convergence of discrete approximations to the Navier–Stokes equations, Math. Comput. 23 (106) (1969) 341–353.
[42] R. Temam, Sur l'approximation de la solution des equations de Navier–Stokes par la méthode des pas fractionnarires II, Arch. Ration. Mech. Anal. 33 (1969) 377–385.
[43] T. Goudon, P.-E. Jabin, A. Vasseur, Hydrodynamic limit for the Vlasov–Navier–Stokes equations. I. Light particles regime, Indiana Univ. Math. J. 53 (6) (2004) 1495–1515.
[44] T. Goudon, S. Jin, J. Liu, B. Yan, Asymptotic-preserving schemes for kinetic-fluid modeling of disperse two-phase flows with variable fluid density, preprint.
[45] F. Filbet, S. Jin, A class of asymptotic-preserving schemes for kinetic equations and related problems with stiff sources, J. Comput. Phys. 229 (20) (2010) 7625–7648.
[46] A. Chorin, Numerical solution of the Navier–Stokes equations, Math. Comput. 22 (104) (1968) 745–762.
[47] J. Kim, P. Moin, Application of a fractional-step method to incompressible Navier–Stokes equations, J. Comput. Phys. 59 (2) (1985) 308–323, http://dx.doi.org/10.1016/0021-9991(85)90148-2.
[48] J. van Kan, A second-order accurate pressure correction scheme for viscous incompressible flow, SIAM J. Sci. Stat. Comput. 7 (1986) 870–891, http://dx.doi.org/10.1137/0907059.
[49] J. Bell, P. Colella, H. Glaz, A second-order projection method for the incompressible Navier–Stokes equations, J. Comput. Phys. 85 (2) (1989) 257–283.
[50] J. Bell, D. Marcus, A second-order projection method for variable-density flows, J. Comput. Phys. 101 (2) (1992) 334–348, http://dx.doi.org/10.1016/0021-9991(92)90011-M.
[51] A. Almgren, J. Bell, P. Colella, L. Howell, M. Welcome, A conservative adaptive projection method for the variable density incompressible Navier–Stokes equations, J. Comput. Phys. 142 (1998) 1–46. <http://dx.doi.org/10.1006/jcph.1998.5890> .
[52] J.-L. Guermond, L. Quartapelle, A projection FEM for variable density incompressible flows, J. Comput. Phys. 165 (2000) 167–188. <http://dx.doi.org/10.1006/jcph.2000.6609> .
[53] C. Calgaro, E. Creusé, T. Goudon, An hybrid finite volume-finite element method for variable density incompressible flows, J. Comput. Phys. 227 (2008) 4671–4696.
[54] A. Quarteroni, R. Sacco, F. Saleri, Numerical Mathematics, 2nd Edition., Springer, Berlin Heidelberg, Germany, 2007.